JACS
JOURNAL OF THE AMERICAN CHEMICAL SOCIETY

Article

pubs.acs.org/JACS

Thermodynamically Guided Synthesis of Mixed-Linker Zr-MOFs with Enhanced Tunability

Shuai Yuan,[†,§] Jun-Sheng Qin,[†,§] Lanfang Zou,[†] Ying-Pin Chen,[†,‡] Xuan Wang,[†] Qiang Zhang,[†] and Hong-Cai Zhou*[,†,‡]

[†]Department of Chemistry, Texas A&M University, College Station, Texas 77843-3255, United States

[‡]Department of Materials Science and Engineering, Texas A&M University, College Station, Texas 77842, United States

Supporting Information

ABSTRACT: Guided by thermodynamics, we have synthesized two mixed-linker zirconium-based metal−organic frameworks (Zr-MOFs), namely, PCN-133 and PCN-134. Both of them possess a layer-pillar structure, in which the connection between Zr_6 clusters and primary BTB linkers form a (3,6)-connected **kdg** layer that is further extended into 3D frameworks by auxiliary DCDPS/TCPP linkers (BTB = benzene tribenzoate, DCDPS = 4,4′-dicarboxydiphenyl sulfone, TCPP = tetrakis(4-carboxyphenyl)porphyrin). PCN-134 demonstrates high porosity (N_2 uptake of 717 $cm^3 \cdot g^{-1}$ and BET surface area of 1946 $cm^2 \cdot g^{-1}$) and excellent chemical stability in aqueous solutions with pH values ranging from 0 to 13. More importantly, PCN-134 tolerates the partial absence of auxiliary linkers leading to structural defects during the assembly process while preserving its framework integrity. Furthermore, the defect density can be systematically controlled by tuning the occupancy of the auxiliary linker, which in turn affects the MOF properties. For instance, the dichromate uptake of PCN-134 is tuned by adjusting the BTB/TCPP ratios, which gives rise to an efficient dichromate absorbent when the TCPP molar ratio in linkers is set as 22%. In addition, the photocatalytic reduction of Cr(VI) in aqueous solution was also performed by PCN-134−22%TCPP which exhibits excellent catalytic activity. This work not only opens up a new synthetic route toward mixed-linker MOFs, but also provides tunable control of MOF defects and, in turn, the properties.

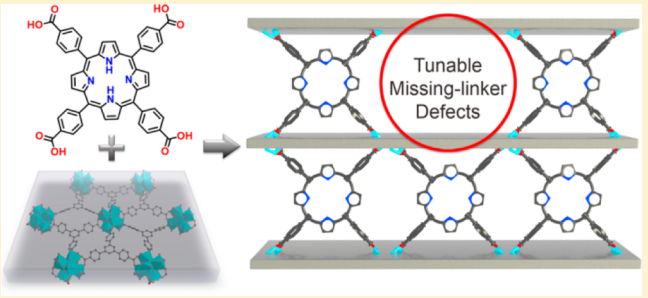

INTRODUCTION

Metal−organic frameworks (MOFs), which are also known as porous coordination networks (PCNs), are an emerging class of porous materials assembled by coordination bonds between metal ions (or clusters) and organic linkers.[1] Owing to their structural and functional tunability, the study of MOFs has become one of the fastest growing research topics in synthetic chemistry and material science. One of the recent MOF synthetic approaches focuses on the creation of "heterogeneity within order,"[2] which integrates multiple synergistic functionalities into one ordered framework. Among them, a common strategy is the utilization of linkers with similar length but distinct functionalities in the construction of mixed-linker MOFs.[3] One of the representative examples is the successful synthesis of multivariate MOFs (MTV-MOFs), demonstrated by Yaghi and co-workers,[3b] in which up to eight linear linkers, each bearing a different functional group, were introduced into one framework. Further efforts were devoted to elucidate the apportionments of functional groups in MTV-MOFs by solid state NMR and molecular simulation. However, it is still tremendously challenging to determine the exact position of each component due to the lack of control over the distribution of the disordered functional groups.[4]

To address this issue, researchers have tried to control the arrangement of functionalities by the introduction of two or more topologically distinct linkers bearing different functional groups.[5] Multiple functional groups were consequently anchored in predefined positions of the MOF pores through the following steps: (i) the linker backbones account for a predetermined topology of framework, and (ii) different linkers are located in predetermined positions in the crystalline lattice. Recently, this has been demonstrated by copolymerization of multiple topologically distinct linkers to produce isoreticular sets of MOFs with systematically modulated pore architectures.[6] So far, this approach has only been shown with soft Lewis acidic metal species (M^{2+}).[5,7] However, the resultant materials usually exhibit relatively poor chemical stabilities, which severely limits their applications.

Owing to its superior stability and tunable connectivity,[8,9] the Zr_6 cluster is considered to be an attractive building block for the preparation of mixed-linker MOFs. Furthermore, Zr-MOFs are known for their extraordinary tolerance of defects,[10] which makes them ideal for the construction of mixed-linker MOFs with various linker ratios. For instance, the linker ratios of these

Received: March 30, 2016
Published: May 6, 2016

DOI: 10.1021/jacs.6b03263
J. Am. Chem. Soc. 2016, 138, 6636−6642

Zr-MOFs can be altered by partially replacing one linker with defects. Likewise, the defect concentration can also be tuned by judicious control of linker ratios. Nevertheless, the one-pot synthesis of Zr-MOFs using multiple linkers of different lengths has seldom been explored.[11] Efforts have been devoted exclusively in our lab to producing mixed-linker Zr-MOFs starting from a combination of linear linkers, but to no avail. In the literature, 12-connected Zr-MOFs with UiO structures are thermodynamically more favored, and thus, UiO structures are generated instead of mixed linker phases.[12]

Our previous work demonstrated that mixed linker Zr-MOFs can be obtained by a kinetically controlled synthetic strategy, namely, *Sequential Linker Installation* (SLI).[11] This strategy utilizes a stable Zr-MOF with inherent coordinatively unsaturated sites as a matrix, and postsynthetically installs linkers with different functionalities and lengths sequentially through kinetic control. In this case, the terminal $-OH^-/H_2O$ ligands capped on the coordinatively unsaturated sites of the Zr_6 cluster were substituted by linear dicarboxylate linkers via an acid–base reaction. However, some potential limitations still remain with this strategy. First, SLI usually requires a complicated procedure and specific control of reaction conditions as a postsynthetic modification strategy. Moreover, it requires extra effort to precisely control the linker ratio and defect concentration since the subsequently installed linker tends to react with all terminal $-OH^-/H_2O$ ligands on the Zr_6 cluster. In this regard, the facile one-pot synthesis of mixed-linker Zr-MOFs is highly desired.

In the light of existing literature and our previous work,[8−11] we proposed a thermodynamically guided strategy for the synthesis of mixed-linker Zr-MOFs. The formation of the Zr–carboxylate bond is an exothermic process, so MOFs with highly connected Zr_6 clusters are thermodynamically favored. This explains why thermodynamically favored high connected UiO structures often prevail in the synthesis of mixed-linker Zr-MOFs directly from linear linkers. To integrate two linkers within a Zr-MOF structure, the linkers must be selected rationally (Scheme 1): with any single linker, it is difficult or

Scheme 1. Thermodynamically Guided Strategy for the Synthesis of Mixed-Linker Zr-MOFs

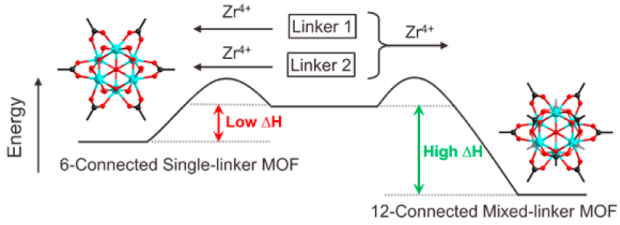

impossible to form 12-connected Zr-MOFs. However, a combination of two linkers should give rise to a highly connected Zr-MOF as a thermodynamically favored product. To demonstrate the effectiveness of our proposed strategy, two mixed-linker Zr-MOFs, namely $Zr_6O_4[OH]_4[BTB]_2[DCDPS]_3$ (PCN-133, BTB = benzene tribenzoate, DCDPS = 4,4′-dicarboxydiphenyl sulfone) and $Zr_6O_4[OH]_6[H_2O]_2[BTB]_2[TCPP]$ (PCN-134, TCPP = tetrakis(4-carboxyphenyl)porphyrin), were synthetically achieved. They show increased porosity and stability compared to the parent MOFs constructed from a single BTB linker. More importantly, the defects of PCN-134 can be controlled by adjusting the linker ratios, which in turn affects its behaviors on the uptake and conversion of $Cr_2O_7^{2-}$ ions in aqueous solutions.

RESULTS AND DISCUSSION

Structural Design. Guided by the thermodynamically controlled synthetic strategy, we seek linkers that cannot form a reasonable structure with 12-connected Zr_6 clusters. To meet such a challenge, BTB was adopted as a primary linker because its geometry does not topologically match with 12-connected Zr_6 cluster.[13] As shown in Figure 1a, the Zr_6 cluster reduces its connectivity to six with a hexagonal shape and is extended by the triangular BTB linker, thus forming a 2D layer with a (3,6)-connected **kdg** topology (Figure 1b). Besides connection with six carboxylate groups within the layer, six pairs of terminal $-OH^-/H_2O$ ligands on the Zr_6 cluster were left above and below the layer, poised for carboxylate linkers. Intuitively, the Zr–BTB layer can be extended into a 3D network by ditopic linkers, which act as pillars to support the layers (Figure 1c). However, the introduction of linear linkers tends to generate 12-connected UiO structures largely driven by thermodynamics.[12,14] A close examination of the Zr–BTB structure reveals that each pair of linkers can be extended with three bent ditopic fragments. Bearing such structural rationalization in mind, we selected a bent ditopic linker, DCDPS. Series of reactions between DCDPS and $ZrCl_4$ were carried out under solvothermal conditions which did not give rise to a crystalline product, possibly due to the incompatible conformation. The DCDPS as an auxiliary linker is expected to form a layer-pillar structure when combined with the Zr–BTB layer. As expected, the reaction between $ZrCl_4$, BTB, and DCDPS gave rise to single crystals of a mixed-linker Zr-MOF with a layer-pillar structure, denoted as PCN-133 (Figures 2c and S1a). With the successful construction of PCN-133, we proposed that tetratopic linkers can also work as pillars to support Zr–BTB layers if they meet the size and topology compatibility. Theoretically, TCPP can be regarded as a combination of two mirror-symmetric DCDPS moieties (Figures 2b and S2). Furthermore, TCPP tends to form porous frameworks with 6- or 8-connected Zr_6 clusters under a wide range of synthetic conditions, which have been reported in previous studies.[9] In a word, TCPP satisfied all the criteria required to construct a mixed-linker Zr-MOF with BTB. To prove our hypothesis, another mixed-linker Zr-MOF, PCN-134 (Figures 2d and S1b), was successfully synthesized with BTB and TCPP as precursors through judicious control of reaction conditions that steered the system toward multicomponent MOFs and away from competing phases.

Structural Description. Single-crystal X-ray analysis revealed that PCN-133 crystallized in the hexagonal space group *P6/mmm* (No. 191, Table S1). The Zr_6 clusters and the BTB linkers are twofold disordered in the solved crystal structure. Note that the disordered Zr_6 clusters have also been encountered in another Zr-MOF with hexagonal crystal system reported by our group.[15] Each individual Zr_6 cluster was connected by six carboxylate groups from six BTB linkers in the *ab*-plane, and each BTB linker was attached to three Zr_6 cores to lead to a 2D layer (Figure S3). The 2D layer was further pillared by DCDPS fragments that linked each pair of Zr_6 clusters from adjacent layers by replacing the terminal $-OH^-/H_2O$ ligands (Figures 2 and S4a). From the topological viewpoint, each Zr–BTB layer can be simplified into a **kgd** net and then extended into a (3,8)-connected **tfz-d** net by DCDPS moieties (Figure S4b).[16]

DOI: 10.1021/jacs.6b03263
J. Am. Chem. Soc. 2016, 138, 6636−6642

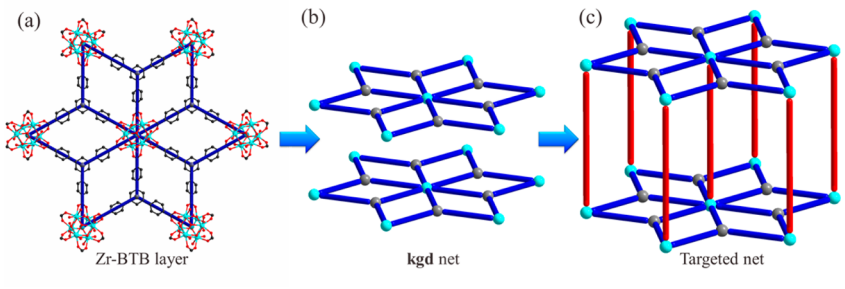

Figure 1. Design of mixed-linker Zr-MOFs: (a) the 2D Zr−BTB layer composed of Zr_6 cluster and primary BTB linker; (b) (3,6)-connected net originated from 2D Zr−BTB layer; and (c) view of layer-pillar structure of (3,6)-connected net supported by another auxiliary linker.

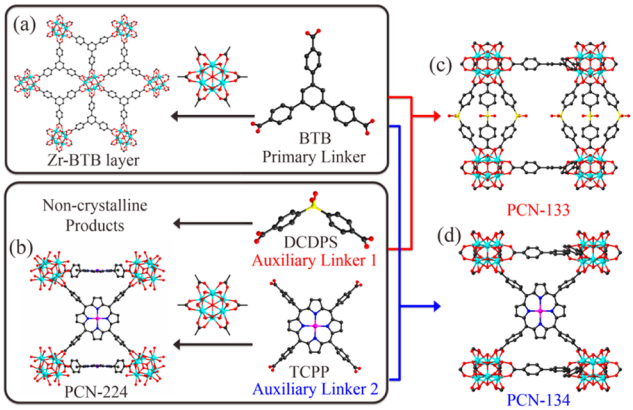

Figure 2. Construction of mixed-linker Zr-MOFs: (a) the 2D Zr−BTB layer formed by 6-connected Zr_6 cluster and BTB; (b) PCN-224 formed by 6-connected Zr_6 cluster and TCPP; (c) PCN-133 formed by 12-connected Zr_6 cluster, BTB, and DCDPS; and (d) PCN-134 formed by 10-connected Zr_6 cluster, BTB, and TCPP.

Reaction of $ZrCl_4$, BTB and TCPP in DMF yields red crystals of PCN-134. The substitution of TCPP by Ni(II)-TCPP under similar conditions further yielded PCN-134(Ni), which was suitable for single crystal X-ray diffraction. Similar to PCN-133, PCN-134(Ni) also crystallized in the space group *P6/mmm* (Table S1). Because of the symmetry of the hexagonal crystal system, the Zr_6 cluster and BTB fragment were also 2-fold disordered in the resolved structure. The Zr_6 clusters were linked with 3-connected BTB fragment into a (3,6)-connected **kdg** net that was further supported by Ni(II)-TCPP linkers to form a 3D layer-pillar structure (Figure 2). To better understand the structure of PCN-134(Ni), an ordered structure was simulated in the orthogonal space group *Imma*. With increased unit cell size and decreased symmetry, the disorder of Zr_6 clusters, BTB, and Ni(II)-TCPP fragments are eliminated. Due to the topological restriction, each cluster is 10-connected with six carboxylates from BTB and four carboxylates from TCPP (Figure S5), leaving two connection sites terminated by $-OH^-/H_2O$ ligands. The occupancy of Ni(II)-TCPP is refined as 1/3, as each cluster is only coordinated with four carboxylates from TCPP fragments and two pairs of terminal $-OH^-/H_2O$ ligands. The linker ratio is consistent with the ^1H NMR results of digested samples. From the topological viewpoint, the Zr−BTB layer was extended by TCPP fragments into a (3,4,10)-connected net with a point symbol of $\{4^{16}.6^{20}.8^9\}\{4^3\}_2\{4^4.6^2\}$ (Figure S6).[17] The samples of PCN-134 with metal-free TCPP linker was confirmed by powder X-ray diffraction (PXRD) and used for the further studies except for defect analysis by chemical titration.

Enhanced Porosity and Stability. The purities of PCN-133 and PCN-134 were confirmed by the comparison of their experimental PXRD patterns and simulated patterns derived from single-crystal X-ray diffraction (Figures 3a and S7). More importantly, PCN-134 exhibits an excellent chemical stability in aqueous solution within a wide range of pH values for 24 h. The chemical stability was evaluated by suspending the as-synthesized samples in HCl or NaOH aqueous solutions at room temperature for 24 h. After the stability test, the samples were thoroughly washed with acetone and dried before characterization. As shown in Figure 3a, the PXRD patterns show the framework of PCN-134 remains intact upon immersion in aqueous solutions ranging from pH = 0 to 13, although slight differences of the peak strength can be observed in the PXRD patterns. Moreover, the N_2 sorption isotherms of

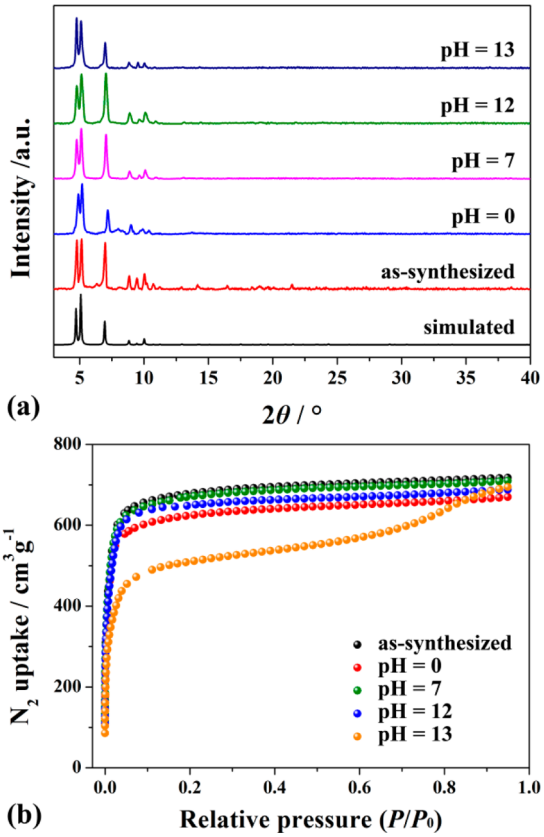

Figure 3. Stability test of PCN-134 (TCPP ratio = 25%): (a) PXRD patterns and (b) N_2 isotherms after immersion in aqueous solutions with different pH values at room temperature for 24 h.

DOI: 10.1021/jacs.6b03263
J. Am. Chem. Soc. 2016, 138, 6636−6642

samples after similar treatment in aqueous solutions confirmed that PCN-134 can survive under these conditions (Figure 3b). These results suggest that no framework collapse or phase transition happens during the stability test. The stability of PCN-133 is relatively lower than PCN-134, possibly due to the hydrophilic $-SO_2$ group and the flexibility of DCDPS linker (Figures S7 and S8).

Compared to the reported Zr-MOFs with 6- or 8-connected Zr_6 clusters (for instance, PCN-222, PCN-224, PCN-225, and PCN-777),[9,18] PCN-134 shows dramatic increased stability, especially in basic media. This is presumably attributed to the highly connected metallic clusters that are highly resistant to the attack of water, acid, and base.[15,19,20] The low connected Zr SBU, with more terminal $-H_2O$ and $-OH^-$ groups on the cluster, is prone to be attacked by acid or base, which is expected to reduce the MOF stability in acidic or basic media. In addition, PCN-134 also exhibits a much improved stability compared to the 2D Zr−BTB MOF, which can be attributed to the fact that the 2D layered structure reduces the rigidity of the whole framework and further influences the stability of the material.[13a] Overall, the increased number of connections and rigid framework accounts for the high stability of PCN-134, which is a prerequisite for practical applications.

The pillar linker opens up the space between each Zr−BTB layer, and therefore, the porosity of PCN-133 and PCN-134 is greatly improved compared to the prototypical MOF (Zr−BTB structure).[13a] In particular, the N_2 uptake of PCN-134 (TCPP ratio = 25%) reaches 717 $cm^3 \cdot g^{-1}$ at 77 K (Figure 3b), which is almost 4 times as much as the prototypical MOF (179 $cm^3 \cdot g^{-1}$).[13a]

Control of Linker Ratio. Different from other mixed-linker MOFs, PCN-134 takes advantage of the nature of Zr-MOFs, possessing high porosity and stability, which allows a high defect density. In this way, the linker ratio can be tuned if auxiliary linker is partially absence. Herein, we explored the possible linker ratios that can be realized within PCN-134 system.

As the linker ratio of reactants would strongly affect the phase purity of the product, we must first optimize the synthetic condition of PCN-134 with different linker ratios. High-throughput methods were employed to study the influence of reaction parameters on the products. The effects of linker ratio and modulating reagent were investigated (Table S2) and summarized into a phase diagram (Figure 4a). The product of each trial was recorded by PXRD to determine the phase purity. At a fixed concentration of modulating reagent (1.7 M), the molar ratio of BTB in the starting material determines the phase purity of the product. When the TCPP is in majority, only a Zr−TCPP-MOF, namely, PCN-224, will be formed.[9b] With an increased BTB ratio, PCN-134 starts to form, while PCN-224 still exists as impurity (Figure S9). When the molar ratio of TCPP decreases to 30%, pure PCN-134 phase is obtained. A further decrease of TCPP ratio does not affect the framework of the PCN-134 phase, which is confirmed by PXRD patterns (Figures 4b and S10). However, it will affect the linker ratios in the final products. The linker ratio of BTB and TCPP in defect free PCN-134 is 2:1, so a pure PCN-134 phase only appears at high ratios of BTB. As shown in Figure S11, the linker ratio in the starting material is proportional to the linker ratio in the PCN-134 as proved by ^1H NMR results.

Furthermore, the concentration of the modulating reagent also has an effect on the phase purity. When the ratio of TCPP is 30%, the product varies from noncrystalline powders to

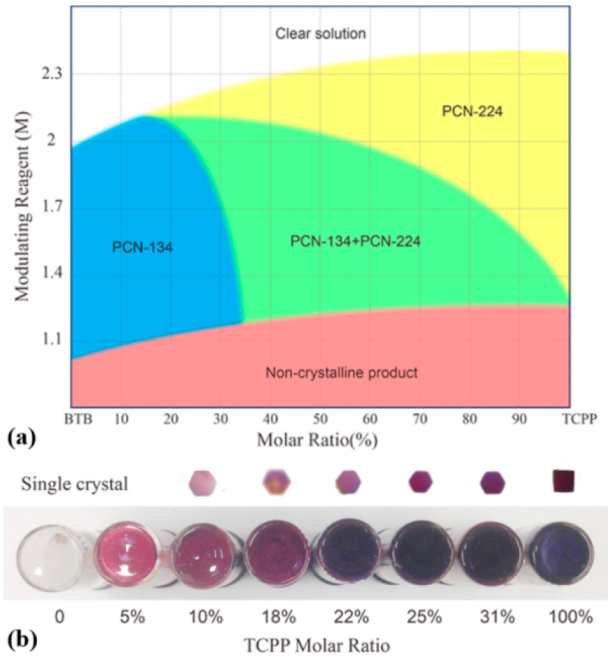

Figure 4. (a) Phase diagram showing the products under different synthetic conditions, and (b) photos of PCN-134 with different TCPP ratios, except for the last one, which is PCN-224.

PCN-134 phase with an increase of modulating reagent. Further addition of modulating reagent gives rise to PCN-224 impurity, as confirmed by subsequent PXRD patterns (Figure S12). The modulating reagent is known to create to the defect sites during the MOF synthesis so that a MOF with low connected Zr_6 clusters (PCN-224) is favored compared to highly connected ones (PCN-134) at elevated modulating reagent concentrations.

Unlike the TCPP system, DCDPS do not form crystalline product with Zr_6 clusters owing to its bent conformation, leading to an easy control of phase purity. The reaction between $ZrCl_4$, BTB, and DCDPS gives a pure product, PCN-133, at a relatively wide range of DCDPS ratios from ∼0.2 to ∼0.8 (Figures S13 and S14).

Control of Defects. A good control of pure PCN-134 phase with different linker ratios makes it possible to study the effects of linker ratios on the MOF properties. In fact, TCPP ratio in the PCN-134 framework can vary from 5% to 31% without changing its structure (Figure S10). We proposed that the TCPP fragment that acted as pillar is partially absent, thereby creating defects. This was further proved by the subsequent N_2 uptake (Figure 5). The simulated N_2 uptake of defect free PCN-134 (i.e., PCN-134-33%TCPP) is 657 $cm^3 \cdot g^{-1}$, which is slightly higher than that of PCN-134-31%TCPP (624 $cm^3 \cdot g^{-1}$). This suggests that PCN-134-31%TCPP is almost defect free. A decrease of TCPP ratio would increase the N_2 uptake: with a TCPP ratio of 25%, PCN-134 has a N_2 uptake of 717 $cm^3 \cdot g^{-1}$, which is even higher than the theoretical value. The BET surface area of PCN-134-25%TCPP was 1946 $cm^2 \cdot g^{-1}$, based on the nitrogen adsorption isotherm. This is possibly caused by the defects between the Zr−BTB layers resulting from missing TCPP fragments, which increases the porosity and decreases the material density. Further decrease of TCPP ratio would decrease the measured N_2 absorbance, possibly resulting from the excess defect that sacrifices the MOF stability and crystallinity. However, as for the PCN-133 system, the

DOI: 10.1021/jacs.6b03263
J. Am. Chem. Soc. 2016, 138, 6636−6642

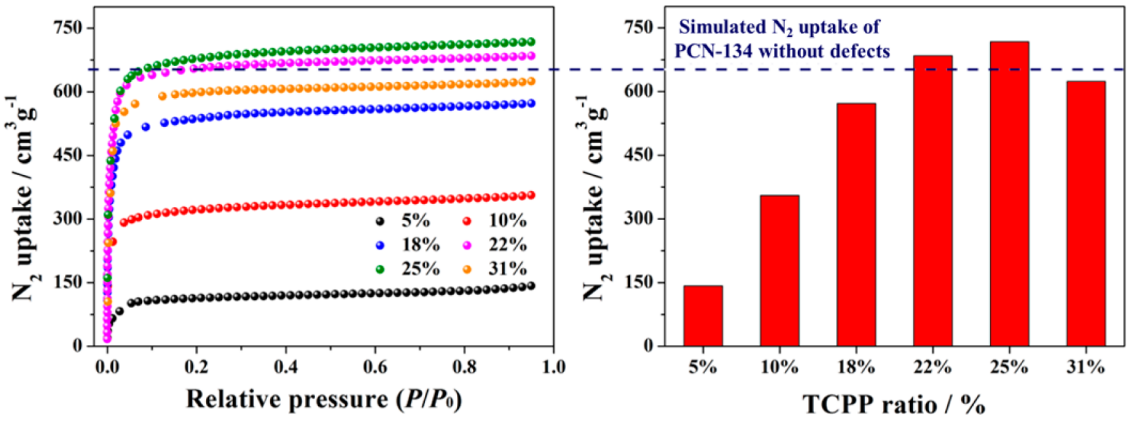

Figure 5. Effects of TCPP defects of PCN-134 system on N_2 uptake measured at 77 K.

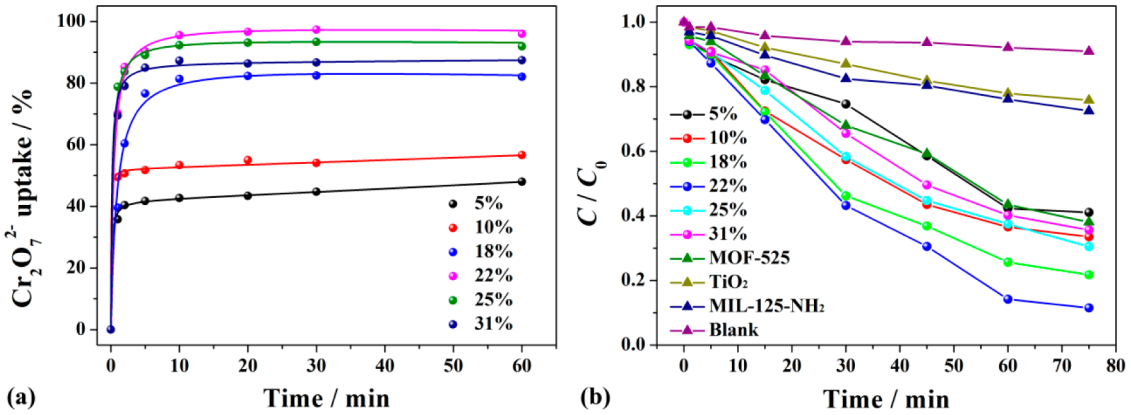

Figure 6. (a) $Cr_2O_7^{2-}$ adsorption capacities and (b) photocatalytic activities for the reduction of $Cr_2O_7^{2-}$ under visible light irradiation of PCN-134 system with different TCPP molar ratios.

more DCDPS defect ratio in the framework, the less nitrogen absorbance of the as-synthesized material (Figure S15). This result might be attributed to the fact that more DCDPS defects in the framework would sacrifice the stability and porosity of the as-synthesized materials considering the flexible nature of DCDPS.

Defect Analysis. According to linker ratio control experiments, TCPP ratio in PCN-134 can be systematically tuned from 5% to 31% and the pillared TCPP linker would partially miss creating defects. It is likely that the defect positions in as-synthesized Zr-MOFs were capped by benzoates, owing to the fact that PCN-134 was synthesized using benzoic acid (BA) as a modulating reagent (Figure S16). Consequently, the defect concentration can be determined by analyzing the concentration of benzoate through ^{1}H NMR technique. This method has been proved to be effective for determining the content of terminal $-OH_2$ and $-OH$ groups in the 8-connected Zr_6 cluster of NU-1000.[21] The as-synthesized samples were washed thoroughly with DMF and then digested by D_2SO_4/DMSO-d_6 for ^{1}H NMR analysis. As described in Figure S17, the BA molar ratio in all the samples increases as the TCPP molar ratio decreases, indicating that the TCPP linkers were replaced by terminal BA ligands to create defects. The experimental values of BA concentration were in agreement with the theoretical ones with slightly lower values within PCN-134 system with different TCPP molar ratios.

Although the exact identity of defect sites in fully activated samples is unknown, the missing auxiliary linkers would most likely be replaced with $-OH_2$ and $-OH$ groups to compensate for the charge loss from the linkers. This is expected to provide extra active protons (Figure S18). Therefore, the active protons can stoichiometrically react with strong base, and thus the defect concentration can be estimated. Inspired by the well-established methods of surface hydroxyl moiety titration in amorphous oxides (such as SiO_2 and TiO_2) as well as in UiO-67,[22,23] we would like to quantitatively characterize the proton concentration by chemical titration. The Ni(II)-TCPP was used to synthesize PCN-134(Ni) in order to eliminate the influence of protons from porphyrin center. Before titration, PCN-134(Ni) samples with different defect density were washed thoroughly with water, DMF, and acetone, and then dried under vacuum to remove the BA and water. The samples were then titrated with an excess of CH_3Li and the amount of evolved methane was quantified by gas chromatographic analysis. The proton concentrations in PCN-134 samples decreased from 7.4 to 3.9 mmol·g^{-1} as the TCPP ratio increased from 10% to 31%, which matched well with the theoretical calculations (Figure S19). It should be noted that titration results should be interpreted cautiously as the stability of samples will also affect the accessibility of active protons. For example, PCN-134-5%TCPP had a much lower proton concentration than expected because of its high defect density and low stability of pore architecture, which possibly collapses and hinders the accessibility of defect sites. Indeed, PCN-134-5%TCPP exhibits low porosity as proven by nitrogen isotherms.

Elimination of Trace $Cr_2O_7^{2-}$ from Water. Hexavalent chromium is classified as a Group "A" human carcinogen by the

DOI: 10.1021/jacs.6b03263
J. Am. Chem. Soc. 2016, 138, 6636−6642

United States Environment Protection Agency, because of its mutagenicity, carcinogenicity, and teratogenicity for human health.[24] It is necessary and essential to completely eliminate $Cr_2O_7^{2-}$ ions prior to wastewater discharge and drinking water distribution. However, it is cumbersome with conventional operation technologies owing to the low adsorption capacities, slow kinetics, and inferior selectivity of traditional materials.[25] Hence, an alternative approach and advanced materials are in demand for the treatment of $Cr_2O_7^{2-}$contamination from water.[26] The missing linker sites in Zr-MOFs are reported to bind strongly with anion such as arsenate and selenate.[27] With controlled missing linker density, tunable porosity, and high chemical stability, PCN-134 is an ideal and attractive platform for the study of $Cr_2O_7^{2-}$ capture.

The performance of PCN-134 in the removal of dichromate from the aqueous solution was studied by placing the dried adsorbent into a dichromate solution (50 ppm). The solution was stirred under ambient temperature, and the $Cr_2O_7^{2-}$ concentration was determined by the UV/vis absorption spectrum at 257 nm. The PCN-134-22%TCPP showed the highest $Cr_2O_7^{2-}$ uptake (Figure 6a): the concentration of $Cr_2O_7^{2-}$ ions decreased by 85% in 2 min and over 95% of dichromate can be removed within 10 min. The terminal $-H_2O/OH$ groups on missing linker defect sites are responsible for dichromate binding. However, the high density of missing linker defects hampers the framework stability, which in turn affects the accessibility of active $-H_2O/OH$ groups on the Zr_6 cluster. This explains the relatively low dichromate uptake in PCN-134-5%TCPP and PCN-134-10% TCPP. PCN-134−22%TCPP represents a delicate balance between stability, porosity, and defects. After $Cr_2O_7^{2-}$ adsorption measurements, the as-synthesized samples were separated by centrifugation and further digested for ICP measurements. The results suggest that absorbed amounts of $Cr_2O_7^{2-}$ measured by ICP were well-matched with the UV data (Table S3 and Figure S21).

Given the high adsorption capacity of PCN-134−22%TCPP, selective adsorption tests were performed for a series of anions. As shown in Figure S22, the adsorption capacity of PCN-134-22%TCPP was maintained even when 2-fold excess moles of disturbing ions (F^-, Cl^-, Br^-, NO_3^-, and SO_4^{2-}) was added, compared with the $Cr_2O_7^{2-}$ adsorption capacity in the absence of disturbing ions. Meanwhile, the XRPD pattern indicates that the network of the best performing material, PCN-134−22% TCPP, was maintained after $Cr_2O_7^{2-}$ adsorption (Figure S23).

Moreover, the photocatalytic reduction of Cr(VI) to Cr(III) was also conducted in aqueous solution with a pH value close to 6.[28] After being stirred for 1 h to reach an adsorption−desorption equilibrium in a dark environment, the suspensions were irradiated by a 300 W Xe lamp with 420 nm cutoff filter. The dichromate concentration was calculated by comparing the UV/vis absorbance (at λ = 257 nm). As shown in Figure 6b and Table S4, PCN-134 with 22% TCPP molar ratio exhibited the highest photocatalytic activity, which is higher than well-known photocatalysts such as TiO_2 and MIL-125-NH_2. It is worth mentioning that the performance of PCN-134 exceeded that of MOF-525, which is also composed of a TCPP linker and a 12-connected Zr_6 cluster, suggesting the positive contribution of defect sites to the catalytic activities. We inferred that the binding of dichromate on the defect sites of Zr_6 clusters facilitates the electron transfer process from photosensitizer to substrates and thus the reduction from Cr(VI) to Cr(III). Based on the experimental data, a tentative mechanism proposed for the photoreduction of Cr(VI) by PCN-134 is described in Figure S24. The porphyrin moieties from the linker were excited by visible light to inject electrons into Zr_6 clusters, yielding $[TCPP]^+$. The binding dichromates on Zr_6 clusters were then reduced by the photoelectron into Cr(III), and the $[TCPP]^+$ was reduced back to TCPP by ethanol. Additionally, the subsequent XRPD pattern suggests that the framework of PCN-134 was still retained after $Cr_2O_7^{2-}$ reduction (Figure S25).

CONCLUSION

In conclusion, we have developed a thermodynamically guided strategy for the synthesis of two mixed-linker Zr-MOFs: PCN-133 and PCN-134. Their 3D layer-pillar structures were built from a 2D **kdg** layer, which consists of Zr_6 clusters and BTBs as the primary linkers, supported by auxiliary DCDPS or TCPP linkers. PCN-134 exhibits high porosity and excellent chemical stability in aqueous solutions with pH scale ranges from 0 to 13. More importantly, the mixed-linker Zr-MOF, PCN-134, has significant tolerance of partial auxiliary-linker absence during the assembly process, leading to a high density of structural defects while preserving the overall structure. In addition, the defect density can be systematically tuned by adjusting the linker ratios, which in turn alters the properties of PCN-134. For instance, PCN-134-25%TCPP exhibits the highest nitrogen uptake and PCN-134-22%TCPP exhibits the highest $Cr_2O_7^{2-}$ absorbance compared with those of other TCPP molar ratios in PCN-134 system. Furthermore, PCN-134-22%TCPP exhibits excellent photocatalytic activity toward the reduction of dichromate in aqueous solution under visible light irradiation. Apart from providing two new mixed-linker Zr-MOFs, the strategy developed herein shall lead to a facile synthesis of a stable Zr-MOF with a controllable defect density, which should extend the application of MOF materials in the near future.

ASSOCIATED CONTENT

Supporting Information

The Supporting Information is available free of charge on the ACS Publications website at DOI: 10.1021/jacs.6b03263.

Materials and instrumentation; experimental details; X-ray crystallography; topological analysis; stability test; control of linker ratio; defect analysis; $Cr_2O_7^{2-}$ adsorption and conversion; additional references (PDF)
Crystallographic details for PCN-133 and PCN-134 (CIF)

AUTHOR INFORMATION

Corresponding Author

*zhou@chem.tamu.edu

Author Contributions

§S.Y. and J.-S.Q. contributed equally.

Notes

The authors declare no competing financial interest.

ACKNOWLEDGMENTS

The gas adsorption−desorption studies of this research were supported by the Center for Gas Separations Relevant to Clean Energy Technologies, an Energy Frontier Research Center funded by U.S. Department of Energy, Office of Science, Office of Basic Energy Sciences under Award Number DE-SC0001015. Structural analyses were supported as part of the

DOI: 10.1021/jacs.6b03263
J. Am. Chem. Soc. 2016, 138, 6636−6642

Hydrogen and Fuel Cell Program under Award Number DE-EE-0007049. S.Y. also acknowledges the Texas A&M Energy Institute Graduate Fellowship Funded by ConocoPhillips. S.Y. would also like to thank Ms. Shanshan Liu for proofreading and helpful discussion.

REFERENCES

(1) (a) Yaghi, O. M.; O'Keeffe, M.; Ockwig, N. W.; Chae, H. K.; Eddaoudi, M.; Kim, J. *Nature* **2003**, *423*, 705. (b) Zhou, H. C.; Long, J. R.; Yaghi, O. M. *Chem. Rev.* **2012**, *112*, 673. (c) Cohen, S. M. *Chem. Rev.* **2012**, *112*, 970. (d) Yoon, M.; Srirambalaji, R.; Kim, K. *Chem. Rev.* **2012**, *112*, 1196. (e) Furukawa, H.; Cordova, K. E.; O'Keeffe, M.; Yaghi, O. M. *Science* **2013**, *341*, 1230444. (f) Li, M.; Li, D.; O'Keeffe, M.; Yaghi, O. M. *Chem. Rev.* **2014**, *114*, 1343. (g) Chen, Y.-P.; Liu, T.-F.; Fordham, S.; Zhou, H.-C. *Acta Crystallogr., Sect. B: Struct. Sci., Cryst. Eng. Mater.* **2015**, *B71*, 613.

(2) (a) Furukawa, H.; Müller, U.; Yaghi, O. M. *Angew. Chem., Int. Ed.* **2015**, *54*, 3417. (b) Tu, B.; Pang, Q.; Ning, E.; Yan, W.; Qi, Y.; Wu, D.; Li, Q. *J. Am. Chem. Soc.* **2015**, *137*, 13456.

(3) (a) Chun, H.; Dybtsev, D. N.; Kim, H.; Kim, K. *Chem. - Eur. J.* **2005**, *11*, 3521. (b) Deng, H.; Doonan, C. J.; Furukawa, H.; Ferreira, R. B.; Towne, J.; Knobler, C. B.; Wang, B.; Yaghi, O. M. *Science* **2010**, *327*, 846. (c) Burrows, A. D. *CrystEngComm* **2011**, *13*, 3623. (d) Wang, C.; Xie, Z.; deKrafft, K. E.; Lin, W. *J. Am. Chem. Soc.* **2011**, *133*, 13445.

(4) Kong, X.; Deng, H.; Yan, F.; Kim, J.; Swisher, J. A.; Smit, B.; Yaghi, O. M.; Reimer, J. A. *Science* **2013**, *341*, 882.

(5) (a) Ma, B.-Q.; Mulfort, K. L.; Hupp, J. T. *Inorg. Chem.* **2005**, *44*, 4912. (b) Koh, K.; Wong-Foy, A. G.; Matzger, A. J. *Angew. Chem., Int. Ed.* **2008**, *47*, 677. (c) Doonan, C. J.; Morris, W.; Furukawa, H.; Yaghi, O. M. *J. Am. Chem. Soc.* **2009**, *131*, 9492. (d) Furukawa, H.; Ko, N.; Go, Y. B.; Aratani, N.; Choi, S. B.; Choi, E.; Yazaydin, A. O.; Snurr, R. Q.; O'Keeffe, M.; Kim, J.; Yaghi, O. M. *Science* **2010**, *329*, 424.

(6) (a) Liu, L.; Konstas, K.; Hill, M. R.; Telfer, S. G. *J. Am. Chem. Soc.* **2013**, *135*, 17731. (b) Liu, L.; Telfer, S. G. *J. Am. Chem. Soc.* **2015**, *137*, 3901.

(7) (a) Dybtsev, D. N.; Chun, H.; Kim, K. *Angew. Chem., Int. Ed.* **2004**, *43*, 5033. (b) Fukushima, T.; Horike, S.; Inubushi, Y.; Nakagawa, K.; Kubota, Y.; Takata, M.; Kitagawa, S. *Angew. Chem., Int. Ed.* **2010**, *49*, 4820. (c) Chevreau, H.; Devic, T.; Salles, F.; Maurin, G.; Stock, N.; Serre, C. *Angew. Chem., Int. Ed.* **2013**, *52*, 5056.

(8) (a) Valenzano, L.; Civalleri, B.; Chavan, S.; Bordiga, S.; Nilsen, M. H.; Jakobsen, S.; Lillerud, K. P.; Lamberti, C. *Chem. Mater.* **2011**, *23*, 1700. (b) Deria, P.; Bury, W.; Hupp, J. T.; Farha, O. K. *Chem. Commun.* **2014**, *50*, 1965. (c) Furukawa, H.; Gándara, F.; Zhang, Y.-B.; Jiang, J.; Queen, W. L.; Hudson, M. R.; Yaghi, O. M. *J. Am. Chem. Soc.* **2014**, *136*, 4369. (d) Cliffe, M. J.; Wan, W.; Zou, X.; Chater, P. A.; Kleppe, A. K.; Tucker, M. G.; Wilhelm, H.; Funnell, N. P.; Coudert, F.-X.; Goodwin, A. L. *Nat. Commun.* **2014**, *5*, 4176.

(9) (a) Feng, D.; Gu, Z.-Y.; Li, J.-R.; Jiang, H.-L.; Wei, Z.; Zhou, H.-C. *Angew. Chem., Int. Ed.* **2012**, *51*, 10307. (b) Feng, D.; Chung, W.-C.; Wei, Z.; Gu, Z.-Y.; Jiang, H.-L.; Chen, Y.-P.; Darensbourg, D. J.; Zhou, H.-C. *J. Am. Chem. Soc.* **2013**, *135*, 17105. (c) Jiang, H.-L.; Feng, D.; Wang, K.; Gu, Z.-Y.; Wei, Z.; Chen, Y.-P.; Zhou, H.-C. *J. Am. Chem. Soc.* **2013**, *135*, 13934.

(10) (a) Wu, H.; Chua, Y. S.; Krungleviciute, V.; Tyagi, M.; Chen, P.; Yildirim, T.; Zhou, W. *J. Am. Chem. Soc.* **2013**, *135*, 10525. (b) Øien, S.; Wragg, D.; Reinsch, H.; Svelle, S.; Bordiga, S.; Lamberti, C.; Lillerud, K. P. *Cryst. Growth Des.* **2014**, *14*, 5370.

(11) Yuan, S.; Lu, W.; Chen, Y.-P.; Zhang, Q.; Liu, T.-F.; Feng, D.; Wang, X.; Qin, J.; Zhou, H.-C. *J. Am. Chem. Soc.* **2015**, *137*, 3177.

(12) Cavka, J. H.; Jakobsen, S.; Olsbye, U.; Guillou, N.; Lamberti, C.; Bordiga, S.; Lillerud, K. P. *J. Am. Chem. Soc.* **2008**, *130*, 13850.

(13) (a) Wang, R.; Wang, Z.; Xu, Y.; Dai, F.; Zhang, L.; Sun, D. *Inorg. Chem.* **2014**, *53*, 7086. (b) Ma, J.; Wong-Foy, A. G.; Matzger, A. J. *Inorg. Chem.* **2015**, *54*, 4591.

(14) (a) Schaate, A.; Roy, P.; Godt, A.; Lippke, J.; Waltz, F.; Wiebcke, M.; Behrens, P. *Chem. - Eur. J.* **2011**, *17*, 6643. (b) Katz, M. J.; Brown, Z. J.; Colon, Y. J.; Siu, P. W.; Scheidt, K. A.; Snurr, R. Q.; Hupp, J. T.; Farha, O. K. *Chem. Commun.* **2013**, *49*, 9449.

(15) Feng, D.; Gu, Z.-Y.; Chen, Y.-P.; Park, J.; Wei, Z.; Sun, Y.; Bosch, M.; Yuan, S.; Zhou, H.-C. *J. Am. Chem. Soc.* **2014**, *136*, 17714.

(16) Hou, J.-J.; Zhang, R.; Qin, Y.-L.; Zhang, X.-M. *Cryst. Growth Des.* **2013**, *13*, 1618.

(17) Blatov, V. A. TOPOS 4.0 Professional, Commission on Crystallographic Computing, IUCr, 2006.

(18) Feng, D.; Wang, K.; Su, J.; Liu, T. F.; Park, J.; Wei, Z.; Bosch, M.; Yakovenko, A.; Zou, X.; Zhou, H.-C. *Angew. Chem., Int. Ed.* **2015**, *54*, 149.

(19) Liu, T.-F.; Feng, D.; Chen, Y.-P.; Zou, L.; Bosch, M.; Yuan, S.; Wei, Z.; Fordham, S.; Wang, K.; Zhou, H.-C. *J. Am. Chem. Soc.* **2015**, *137*, 413.

(20) (a) Guillerm, V.; Weseliński, Ł. J.; Belmabkhout, Y.; Cairns, A. J.; D'Elia, V.; Wojtas, Ł.; Adil, K.; Eddaoudi, M. *Nat. Chem.* **2014**, *6*, 673. (b) Xue, D.-X.; Belmabkhout, Y.; Shekhah, O.; Jiang, H.; Adil, K.; Cairns, A. J.; Eddaoudi, M. *J. Am. Chem. Soc.* **2015**, *137*, 5034. (c) Assen, A. H.; Belmabkhout, Y.; Adil, K.; Bhatt, P. M.; Xue, D.-X.; Jiang, H.; Eddaoudi, M. *Angew. Chem., Int. Ed.* **2015**, *54*, 14353. (d) Alezi, D.; Peedikakkal, A. M. P.; Weseliński, Ł. J.; Guillerm, V.; Belmabkhout, Y.; Cairns, A. J.; Chen, Z.; Wojtas, Ł.; Eddaoudi, M. *J. Am. Chem. Soc.* **2015**, *137*, 5421.

(21) Deria, P.; Mondloch, J. E.; Tylianakis, E.; Ghosh, P.; Bury, W.; Snurr, R. Q.; Hupp, J. T.; Farha, O. K. *J. Am. Chem. Soc.* **2013**, *135*, 16801.

(22) (a) Mueller, R.; Kammler, H. K.; Wegner, K.; Pratsinis, S. E. *Langmuir* **2003**, *19*, 160. (b) Setyan, A.; Sauvain, J. J.; Rossi, M. J. *Phys. Chem. Chem. Phys.* **2009**, *11*, 6205.

(23) Larabi, C.; Quadrelli, E. A. *Eur. J. Inorg. Chem.* **2012**, *2012*, 3014.

(24) Testa, J. J.; Grela, M. A.; Litter, M. I. *Environ. Sci. Technol.* **2004**, *38*, 1589.

(25) (a) Prasanna, S. V.; Kamath, P. V. *Solid State Sci.* **2008**, *10*, 260. (b) Li, L.; Fan, L.; Sun, M.; Qiu, H.; Li, X.; Duan, H.; Luo, C. *Colloids Surf., B* **2013**, *107*, 76. (c) Gherasim, C.-V.; Bourceanu, G. *Chem. Eng. J.* **2013**, *220*, 24.

(26) Gutov, O. V.; Hevia, M. G.; Escudero-Adán, E. C.; Shafir, A. *Inorg. Chem.* **2015**, *54*, 8396.

(27) (a) Wang, C.; Liu, X.; Chen, J. P.; Li, K. *Sci. Rep.* **2015**, *5*, 16613. (b) Howarth, A. J.; Katz, M. J.; Wang, T. C.; Platero-Prats, A. E.; Chapman, K. W.; Hupp, J. T.; Farha, O. K. *J. Am. Chem. Soc.* **2015**, *137*, 7488.

(28) (a) Shen, L.; Liang, S.; Wu, W.; Liang, R.; Wu, L. *Dalton Trans.* **2013**, *42*, 13649. (b) Wang, H.; Yuan, X.; Wu, Y.; Chen, X.; Leng, L.; Zeng, G. *RSC Adv.* **2015**, *5*, 32531.

DOI: 10.1021/jacs.6b03263
J. Am. Chem. Soc. 2016, 138, 6636−6642